

Article

Measurement of Air Layer Thickness under Multi-Angle Incidence Conditions Based on Ultrasonic Resonance Reflection Theory for Flange Fasteners

Fei Shang ¹ , Bo Sun ¹  and Honghui Zhang ^{1,2,*} 

¹ School of Mechanical Engineering, Inner Mongolia University of Science and Technology, Baotou 014000, China

² National Engineering Research Center of Flat Rolling Equipment, Beijing University of Science and Technology, Beijing 102200, China

* Correspondence: tygcshi@163.com

Abstract: During the servicing of flange fasteners, the sealing gasket and the flange cover interface are prone to separation and air contamination due to factors such as stress, corrosion, and vibration. In the detection process, there are two main issues: firstly, the conventional ultrasonic measurement methods based on the theory of acoustic elasticity are not applicable due to the small thickness of the air layer; secondly, the use of conventional vertical incidence detection methods is difficult to ensure due to the influence of the actual structure. To address these issues, this paper first establishes a mathematical model of ultrasonic resonance reflection, and then calculates the corresponding relationship between the air layer thickness and the resonance frequency under vertical incidence conditions. However, this model is difficult to use to calculate the resonance frequency under different incidence angles. To meet the requirements of different working conditions, a finite element simulation model is further established. By comparing the calculation results of the two models under vertical incidence, the reliability of the established finite element model is verified. The reflection and transmission pressure acoustic field distribution under different incidence angles and air layer thicknesses is simulated, and the function relationship between the incidence angle, air layer thickness, and the corresponding first-order resonance frequency is derived. This enables the measurement of the air layer thickness at any incidence angle, providing technical and theoretical support for practical industrial applications.

Keywords: air layer thickness; first harmonic resonant; multi-angle incidence; ultrasonic reflection coefficient



Citation: Shang, F.; Sun, B.; Zhang, H. Measurement of Air Layer Thickness under Multi-Angle Incidence Conditions Based on Ultrasonic Resonance Reflection Theory for Flange Fasteners. *Appl. Sci.* **2023**, *13*, 6057. <https://doi.org/10.3390/app13106057>

Academic Editor: Mário João S. F. Santos

Received: 12 April 2023

Revised: 8 May 2023

Accepted: 12 May 2023

Published: 15 May 2023



Copyright: © 2023 by the authors. Licensee MDPI, Basel, Switzerland. This article is an open access article distributed under the terms and conditions of the Creative Commons Attribution (CC BY) license (<https://creativecommons.org/licenses/by/4.0/>).

1. Introduction

Flange fasteners are a common type of mechanical connector for pipes, consisting of a flange cover, a sealing gasket, and fastening bolts, mainly used for shut-off and sealing treatment at the end of pipes, as shown in Figure 1. As flange structures are used in pipeline structures transporting high-pressure fluids, the contact surface requires high sealing performance and therefore needs to be regularly inspected. The pressure of some pipeline containers can reach 90 MPa, and impurities such as chlorides, sulfides, and gravel in the transported medium can easily corrode the surface of the flange and the sealing gasket, resulting in separation between the flange cover and the sealing gasket. When the air layer at the contact interface reaches the critical state, the leaked medium, due to high pressure and temperature, can cause significant impacts on human health and the environment [1,2]. Therefore, it is necessary to regularly inspect the flange structure. Ultrasonic non-destructive testing (NDT) technology is a technique with strong penetration ability, high sensitivity, and non-invasive characteristics, and is therefore widely used for detecting separation defects at contact interfaces [3]. Considering that the thickness

of the air layer at the contact interface is small, the pulse-echo method is not applicable. Currently, many researchers use the finite element method to calculate the ultrasonic reflection coefficient between multi-layer media and characterize the interface contact state according to this acoustic characteristic parameter. Therefore, it can be inferred that the value of the contact stress at the interface can be expressed by the change in the ultrasonic reflection coefficient, and can further express the thickness of the air layer at the contact interface.



Figure 1. Flange fastening device: (a) disassembled, (b) assembled.

Ishii et al. [4] established a power-law relationship between contact stiffness and contact pressure based on extensive experiments, laying the foundation for establishing the relationship between ultrasonic reflection coefficients and contact stiffness. They conducted theoretical analysis and detection experiments on the aluminum–aluminum contact interface state, establishing the relationship between ultrasonic reflection and transmission coefficients and the change in epoxy layer contact stiffness, indicating that solid contact stiffness changes can be characterized by ultrasonic reflection coefficients. Drinkwater et al. [5] studied the detection problem of the compressive interface state of the aluminum–aluminum interface. They assumed that the reflection coefficient of the contact sample was a function of contact stiffness and frequency, and found that the change in the reflection coefficient during unloading was significantly lagging compared to the loading process in cyclic loading–unloading experiments, indicating that the acoustic reflection coefficient was extremely sensitive to changes in load. Wu Wenlin et al. [6] established a reflection and transmission physical model in an air-coupled ultrasonic oblique incidence double-layer adhesive structure based on the wave equation and the simplified spring theory model of interface bonding, using the displacement and stress continuity boundary conditions of ultrasonic waves at each medium interface. They analyzed the change in the transmission coefficient peak value with the interface stiffness coefficient, indicating the effectiveness of acoustic reflection technology in measuring solid bonding surfaces. Zilidou et al. [7] analyzed the acoustic reflection echo on the surface of composite materials and used advanced signal processing techniques to analyze the corresponding signals of the upper and lower surfaces of the material in pulse echo mode, indicating that using pulse-echo technology can simplify the acoustic reflection measurement of multilayer structures. Wang et al. [8] studied the method of evaluating the strength of adhesive structures using air-coupled ultrasonic technology and established the relationship between the sound transmission coefficient, the acoustic resonance frequency, and the type and thickness of the adhesive material by analyzing the changes in the transmission coefficient of different adhesive layers. Li Xiang et al. [9] referred to acoustic principles to analyze the relationship between oil film thickness and reflection coefficient in multilayer media, established COMSOL finite element simulation models with different physical properties and calculating the interface reflection coefficient through standing wave theory. They found that the theory and experimental models were in good agreement, indicating

that fluid layer thickness can be measured with acoustic reflection technology, providing some technical guidance for measuring air layer thickness in subsequent measurements. Geng et al. [10] successfully measured the thickness of layered materials using the phase of the ultrasonic reflection coefficient spectrum and the particle swarm optimization inversion algorithm, demonstrating the application of the ultrasonic reflection coefficient in material thickness measurement. Pan et al. [11] successfully measured the thickness of porous material coatings using ultrasonic complex reflection coefficients, successfully applying acoustic reflection coefficients in engineering measurements. Currently, domestic and foreign scholars mainly analyze the change in interface acoustic reflection coefficients under different contact states based on the acoustic theory between multilayer media [12]. With the continuous development of acoustic and finite element theories, the coupling calculation of multiple physical fields in finite element simulation software is more accurate and efficient, enabling acoustic reflection technology to be widely used in engineering practice.

The previous studies were mainly conducted under the condition of vertical incidence. However, in practical industrial applications, it is difficult to ensure the vertical contact between the ultrasonic transducer and the tested workpiece due to mechanical structure and working environment constraints. As a result, the incidence angle varies with different working conditions. To enhance adaptability, it is necessary to establish a functional relationship between the air gap thickness and the resonant frequency at any incident angle. This can help to overcome the limitations of vertical incidence and provide more flexible and accurate measurements in non-destructive testing for mechanical engineering, acoustics, and other related fields. This article proposes a multi-angle incidence measurement method suitable for practical engineering applications based on previous research on the measurement method of the reflection coefficient, which greatly solves the inconvenience caused by the geometric dimensions and positions of the objects being tested. This study focuses on the separation state of the interface between the flange cover and the silicone sealing gasket in the flange fastening device, and establishes a finite element simulation model for vertical incidence. The first-order resonance frequency under different air layer thicknesses is solved by the theory of sound reflection, and the results show good consistency between theoretical calculations and finite element simulation results, indicating the effectiveness of the vertical incidence finite element simulation model. Furthermore, a multi-angle incidence measurement simulation model is established, and analytical expressions for the air layer thickness and its first-order resonance frequency under different incidence angles are derived to verify the reliability of the multi-angle incidence measurement model, providing a new approach for subsequent practical engineering testing methods.

2. Establishment of the Mathematical Model

Figure 2 shows the ultrasonic reflection/transmission model of the flange fastening device in air, which is mainly composed of Q235 and rubber materials and vertically stacked on a horizontal plane. The first and fifth layers of the structure are Q235, the second and fourth layers are air layers, and the third layer is silicone rubber. To reduce the computational complexity of the model, the influence of roughness on the reflection coefficient has not been considered. In the model, the upper and lower layers are solid materials, and there is a gas layer sandwiched between the solid–solid layers. When the sound wave is incident into the medium at an oblique angle, reflection occurs in the upper solid–gas layer and transmission occurs in the lower solid–gas layer.

According to the theory of acoustic reflection, the acoustic reflection coefficient is related to the density, sound speed, thickness, and acoustic impedance properties of the intermediate layer and the two-sided media. In the contact separation process of the flange fastening device, the thickness of the air layer changes in the range of 10–110 μm . Based on the stress and strain continuity at the boundaries of the multilayer media, the first-order resonance model can be used to accurately predict the ultrasonic reflection coefficient between different thicknesses and different material media.

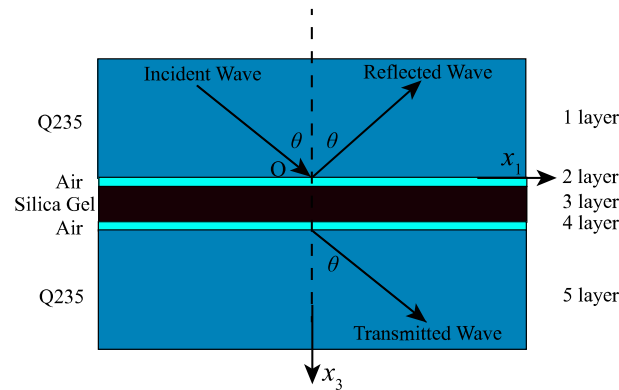


Figure 2. Flange fastening device acoustic reflection/transmission diagram.

When the thickness of the internal air layer is significant in a flange fastening device, its volume and mass cannot be neglected and a first-order resonant model is typically used to measure the air layer thickness [13]. When the sound field is perpendicular to the surface, the reference displacement-stress formula and the continuity boundary conditions of acoustic displacement and stress at the interface can be applied to derive the analytical expression of the ultrasound reflection coefficient R .

In a solid medium, the displacement and stress equations for longitudinal waves are given by [14]:

$$u(x) = Ae^{i\omega x/c} + Be^{-i\omega x/c} \tag{1}$$

$$\sigma(x) = E \frac{\partial u}{\partial x} = i\omega z (Ae^{i\omega x/c} - Be^{-i\omega x/c}) \tag{2}$$

where u is the displacement of the sound wave in the x -direction, σ is the stress induced by the sound wave in the x -direction, A is the amplitude of the incident sound wave, B is the amplitude of the reflected sound wave, ω is the angular frequency, c is the speed of sound in the medium, and $c = \sqrt{E/\rho}$, where ρ is the density of the medium, and z is the acoustic impedance of the medium, $z = \rho c$.

Neglecting the effect of surface roughness on the metal material, the contact between Q235 and the air layer can be regarded as a perfect interface, so the displacement and stress are continuous when crossing the interface.

Therefore, the continuity conditions at $x = 0$ and $x = h$ for the interface are given by:

$$\begin{aligned} u_1|_{x_3=0} &= u'_1|_{x_3=0} \\ \sigma_{33}|_{x_3=0} &= \sigma'_{33}|_{x_3=0} \\ u_3|_{x_3=h} &= u'_3|_{x_3=h} \\ \sigma_{31}|_{x_3=h} &= \sigma'_{31}|_{x_3=h} \end{aligned} \tag{3}$$

where h is the thickness of the air layer.

When assuming the amplitude of the incident wave is 1, Equations (1)–(3) yield [15,16]:

$$R = \frac{g^2(z_2 - z_3)(z_1 + z_2) + (z_1 - z_2)(z_2 + z_3)}{(z_2 + z_3)(z_1 + z_2) + g^2(z_2 - z_3)(z_1 - z_2)} \tag{4}$$

where g has no physical meaning in the equation, $g = e^{i\omega h/c}$, z_i is the acoustic impedance of Q235, air, and silicone, and its calculation formula is $z_i = \rho_i c_i$, ρ_i is the material density, c_i is the internal sound velocity of the material, and $i = 1, 2, 3$.

According to the principles of acoustics, when the thickness of the air layer is a multiple of $\lambda/2$ (λ is the wavelength), a standing wave will occur at the middle position of the air layer where the incident and reflected waves superimpose. The standing wave will cause resonance phenomena, and resonance will occur when the frequency of the ultrasonic wave

is equal to the natural frequency of the air layer [17]. The expression for the resonance angular frequency is:

$$\omega = \frac{\pi cn}{h} \quad (5)$$

The analytical expression for calculating the thickness of the air layer can be obtained after transformation:

$$h = n \cdot \frac{\lambda}{2} = \frac{nc}{2f_n} \quad (6)$$

where n is a positive integer representing the order of resonance, and f_n is the resonant frequency of the n th order.

According to Equation (4), it is known that the reflection coefficient function R is a function of the frequency when the air layer thickness is constant. Assuming that layers 1 and 5 of the medium are Q235 and layers 2 and 4 are air, the relationship between the incident frequency and the reflection coefficient can be calculated under different air layer thickness conditions by looking up the density and sound speed of Q235 and air.

By using Formula (4) and calculating the results based on the data in Table 1, the relationship between incident sound wave frequency and reflection coefficient under different air layer thicknesses can be obtained, as shown in Figure 3. The analysis of Formula (4) reveals that when there is a large difference in density between the media, there may be some errors in the calculated results. As the density of the medium gradually increases, the model error decreases and the change in reflection coefficient is independent of density. Therefore, Formula (4) can be used to analyze the resonant frequency of ultrasound in the air layer and to analyze the thickness of the air layer.

Table 1. The physical parameters of the medium.

Medium	Density (kg/m ³)	Sound Velocity or Speed of Sound (m/s)
Q235	7850	5890
Air	1.29	340
Silicone Gel	1200	2300

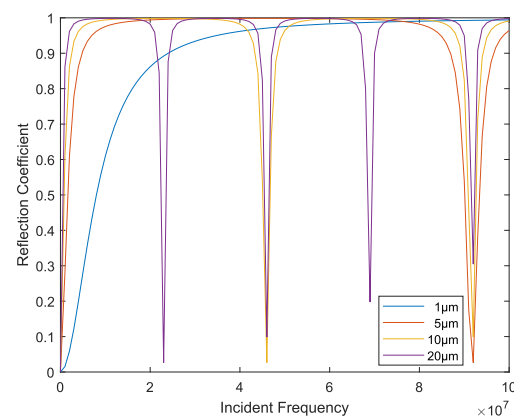


Figure 3. Graph of the relationship between incident frequency and reflection coefficient.

As shown in Figure 3, when the incident frequency of ultrasound is at a specific set of values, the reflection coefficient of the air layer reaches a minimum value. This means that at this incident frequency, the air layer medium resonates with the ultrasound, resulting in a minimum value of the interface reflection coefficient. Therefore, in practical measurements, the thickness of the air layer can be calculated by extracting the resonant frequency corresponding to the minimum value of the reflection coefficient and combining it with Formula (6). Since the reflection coefficient minimum value corresponding to the first-order resonant frequency is easy to select in the calculation process, it is chosen as the reference value.

3. Establishment of the Finite Element Model and Simulation Results

3.1. Establishment of the Finite Element Model

During long-term service, the flange fastening device undergoes a transition from tight contact to small-scale separation between the flange cover and the silicone gasket. During the separation process, the contact interface is prone to air medium intrusion, forming a Q235–air–silicone multi-medium combination. With the aid of COMSOL multiphysics simulation software, a two-dimensional frequency domain analysis model of the multilayer media under a liquid immersion environment is established, as shown in Figure 4. In the figure, \mathbf{k} is the incident wave vector, θ is the angle between the acoustic field and the axis, and I is the contact interface between each medium, where interface I_a and I_d are liquid–solid interfaces and interfaces I_b and I_c are solid medium contact interfaces. The calculation interface used in the simulation process is the acoustic-solid module, where the acoustic analysis is performed using the pressure acoustics module. The fluid domain in the model is solved by calculating the Helmholtz equation in the pressure acoustics module, and the solid domain is solved by calculating Hooke’s law in the solid mechanics module. Once the material parameters in the model are assigned, the material parameters in the subsequent mathematical analysis should be consistent with those in the model. The upper and lower ends of the solid model are set as water domains with a density of 1000 kg/m^3 and a longitudinal wave speed of 1490 m/s [18]. The upper water domain is set as a plane wave with an incident pressure of 1 Pa as the background pressure field for the sound wave incident source.

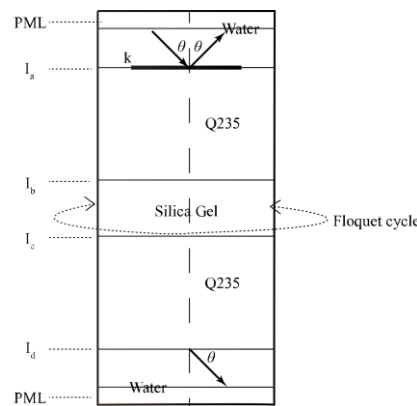


Figure 4. Schematic of the finite element model.

Assuming that the wave vector of the incident plane wave is \mathbf{k} , and it propagates along the incident angle θ to the surface of the flange cover, the expression for wave vector \mathbf{k} is as follows [19,20]:

$$\mathbf{k} = k_0(\sin(\theta) - \cos(\theta)) \tag{7}$$

$$k_0 = \omega / c \tag{8}$$

where ω represents the angular frequency, $\omega = 2\pi f$.

The mathematical definition of the wave vector \mathbf{k} of the incident plane wave is shown below.

$$P_{in}(\mathbf{x}) = 1Pa \cdot \exp(-i(\mathbf{k} \cdot \mathbf{x})) \tag{9}$$

where $\mathbf{x} = (x, y)$, and the wave vector and incident wave are defined as variables in this multi-medium structure model.

Due to the complexity of the incident sound wave after reflection and transmission, the reflection coefficient R is plotted for different combinations of incident angle and frequency (model parameters). The composite ratio of the reflected wave and incident wave at the

multi-layer medium interface is the reflection coefficient, which can be obtained using the following formula [21]:

$$R = \frac{P_{sc}}{P_{in}} = \frac{P_{tot} - P_{in}}{P_{in}} \quad (10)$$

where P_{sc} is the scattered pressure field on the interface I_a in the water, P_{tot} is the transmitted pressure field, and P_{in} is the incident pressure field in the water region on the interface I_a . By using the average value of the reflection coefficient on the multi-layered interface, and matching with different combinations of excitation frequency f and incident angle θ , the variation of the interface reflection coefficient with incident angle and excitation frequency can be calculated. This model reflects the variation in reflection and transmission coefficients of the flange cover and silicone gasket on the flange bolted joint from a state of tight contact to separation, in order to analyze the contact condition of flange fasteners in practical engineering applications.

When the flange fastening device separates from the contact interface, a finite element simulation model can be established with different thicknesses of air layer media (0 μm , 30 μm , 50 μm , 70 μm , 90 μm , 110 μm) on interface I_b . Different characteristic impedances are used to define the media on both sides of the interface, and the characteristic impedance of a material is generally characterized by its density and sound speed.

To eliminate the multiple reflection and refraction effects of acoustic waves at the boundaries of the finite element model and reduce their impact on the calculation results, perfect matching layers (PML) are set at the top and bottom boundaries of the model. The thickness of the PML in the fluid domain is set to 1/3 wavelengths to completely absorb the reflected and transmitted acoustic fields from interface I_a and I_d [22]. To reduce the influence of the reflected and refracted acoustic waves at the left and right boundaries on the post-processing results, Floquet periodic boundary conditions are added to the left and right boundaries of the model to simulate the infinite extension of the calculation model in the horizontal direction [23]. This condition greatly reduces the simulation calculation workload without sacrificing simulation accuracy [24].

To obtain accurate numerical solutions of the model at all frequencies under study, the geometry of the periodic unit cell was set to depend on the wavelength. This means that the geometry was frequency-dependent, which is not allowed in the frequency-domain solver of COMSOL Multiphysics. To avoid this issue, a parametric scan was added, where the scan parameter was the frequency, in order to obtain the frequency and angle spectra of the acoustic reflection coefficient.

During the process of finite element mesh generation, it is necessary to partition the mesh according to the sound speed of different media and the contact position between the media. Therefore, a reasonable refinement of the mesh is needed at each contact interface. Due to the introduction of periodic boundary conditions, the same mesh partitioning method is required at the symmetric boundary. In finite element simulation calculations, the cell partitioning is based on maximizing the computational efficiency while ensuring the calculation accuracy. The PML was set to have a thickness direction "mapping" distribution with 20 layers of elements. Considering the regular shape of the model, no stress changes, and the contact between solids, a free triangular mesh was chosen. According to the Courant–Friedrichs–Lewy (CFL) condition [25], the time step in finite element analysis must be smaller than a certain value, otherwise incorrect calculation results will be obtained. Therefore, the calculation step size of the incident sound wave must be smaller than the time it takes for the sound wave to propagate to adjacent meshes. As the mesh size decreases, the time step also decreases. The Courant–Friedrichs–Lewy condition in two-dimensional space is shown as follows.

$$C = \Delta t \sum_{i=1}^n \frac{u_{xi}}{\Delta x_i} \leq C_{\max} \quad (11)$$

where C is the CFL number, which is a dimensionless quantity. C_{\max} is the maximum CFL value, which indicates that the step displacement of the sound wave in unit time cannot

exceed the unit length of the computational mesh. Generally, $C_{\max} = 1$. Δt is the time step, Δx is the mesh length, and u is the speed of sound wave.

It should be considered that in finite element calculations, computational efficiency needs to be maximized while ensuring the convergence of the calculation. From Equation (11), the relationship between any mesh size and time step can be obtained. Since the water mainly acts as a coupling medium and an absorbing medium, the mesh size can be appropriately increased to reduce the calculation time. As shown in Figure 5 [26], when the mesh size was between $1/6$ and $1/5$ of the wavelength, the relative error of the calculation results changed relatively smoothly. Taking into account the relative error and calculation time, the mesh size was taken to be $1/5$ of the wavelength. The mesh between the contact areas of the various layers of media needed to be appropriately reduced because the sound wave reflection and transmission on the contact surface needed to be calculated with high precision. When the mesh size was less than $1/10$, the relative error approached 0. Taking into account the calculation time, the mesh size was taken to be $1/10$ of the wavelength.

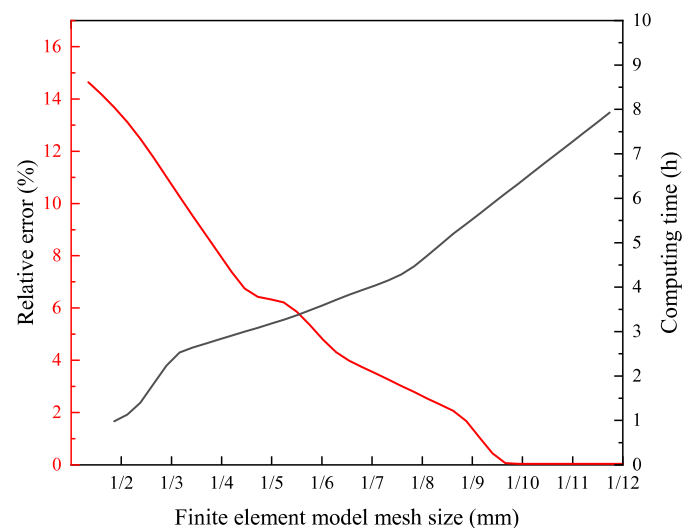


Figure 5. The influence of relative error and calculation time on mesh size [26]. Adapted with permission from Ref. [Research on Ultrasonic Testing Method of Adhesive Quality of Multilayer Structure Based on COMSOL]. 2021, Jiatong Liu.

3.2. Finite Element Simulation Results

The main focus of finite element simulation in this study is the contact behavior between the upper flange and the silicone gasket. Therefore, only the simulation results of the contact interface between the upper flange and the silicone gasket have been selected for data processing and analysis. Through the vertical incidence measurement model, a multi-angle incidence measurement model has been derived and its accuracy proven.

3.2.1. Vertical Incident Simulation Results

Taking the Q235-rubber structure with a single air layer as an example, the reflection characteristics of the air layer under different incident conditions were analyzed using the finite element model shown in Figure 4. The frequency of the incident sound wave was set to 1 MHz, and the incident angle was set to 90° . The parameter scan function was used to set the angle scanning range from 0 to 90° and the frequency scanning range from 0 to 2 MHz.

When the incident wave enters the upper surface of the flange perpendicularly through the background pressure field, part of the sound waves will be scattered, and most of the sound waves will penetrate into the flange, as shown in Figure 6, which shows the sound field maps of the background pressure field and the interface reflection sound field map, respectively.

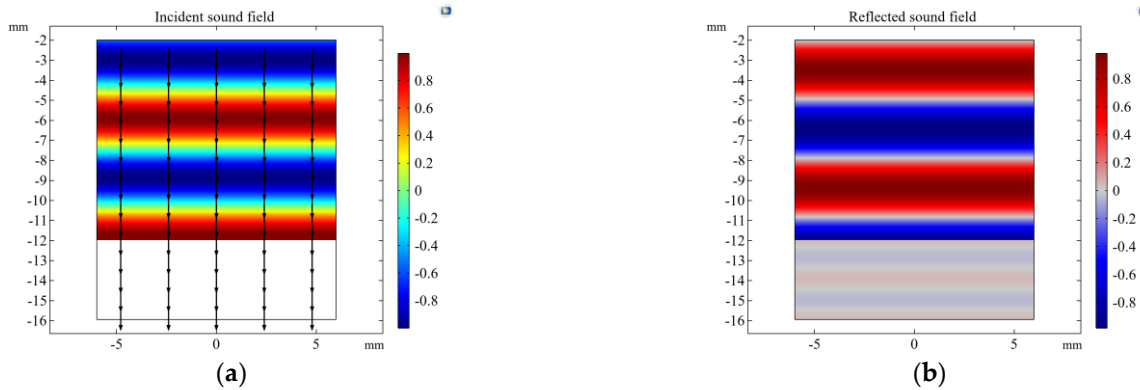


Figure 6. $f = 1 \text{ MHz}$, $\theta = 0^\circ$. Acoustic field map: (a) incident sound field, (b) reflected sound field.

From Figure 6, it can be seen that the maximum sound pressure amplitude of the incident wave is 1 and it enters the upper flange to form a standing wave. The arrow indicates the incident angle of the sound field. When the incident sound field of the upper flange enters the silicone gasket, scattering and transmission occur. When the sound wave propagates in the upper flange, a small amount of sound waves undergo transmission, and most of the sound waves undergo reflection, which is consistent with the actual situation.

Set the thickness of the air layer as $0 \text{ }\mu\text{m}$, $30 \text{ }\mu\text{m}$, $50 \text{ }\mu\text{m}$, $70 \text{ }\mu\text{m}$, $90 \text{ }\mu\text{m}$, and $110 \text{ }\mu\text{m}$. Since the reflected wave is greatly attenuated in the air layer, it is necessary to use the ratio of the incident signal to the reflected signal of the flange and the silicone gasket to determine the reflection coefficient when the incident wave amplitude cannot be determined. A corresponding vertical incidence measurement simulation model is established, and the relationship between the ultrasonic reflection coefficient and the frequency under different air layer thicknesses and incident angles is plotted, as shown in Figure 7.

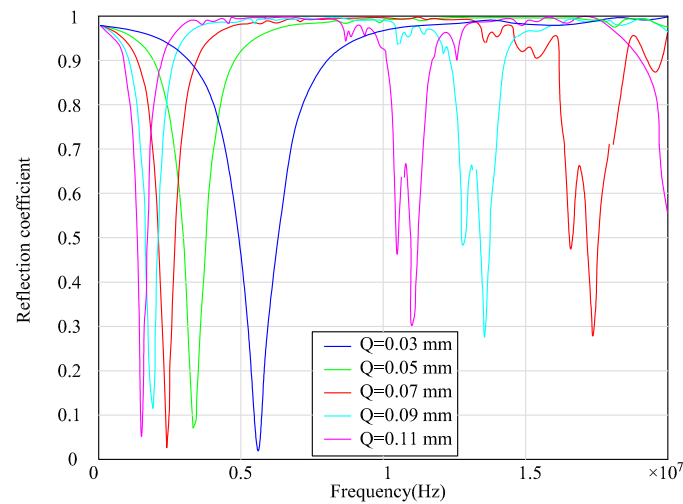


Figure 7. Vertical incidence measurement model reflection coefficient curve.

The above figure shows that there is a clear regularity between different air layer thicknesses and their resonance frequencies. When the air layer thickness increases, the minimum value of the first-order resonance frequency shifts towards the low-frequency direction. As the separation distance between the flange and the silicone gasket increases, the shift amount of the first-order resonance frequency minimum value becomes larger. Therefore, it is feasible to analyze the contact state between the silicone gasket and the flange by analyzing the trend of the minimum value of the resonance frequency.

3.2.2. Simulation Results of Multi-Angle Incident

In most cases, the operating environment of the flange device is complex, and it is difficult for the ultrasonic probe to be perpendicular to the flange surface. Moreover, the placement of the probe is often limited by the size of the flange. Under these circumstances, it is necessary to change the incident angle of the ultrasonic probe to achieve optimal detection results. When the incident wave enters the surface of the flange cover at an angle of 40° through the background pressure field, reflection and projection phenomena occur at the interface between the flange cover and the silicone gasket. As shown in Figure 8, the figures depict the sound field of the background pressure field and the reflected sound field at the interface.

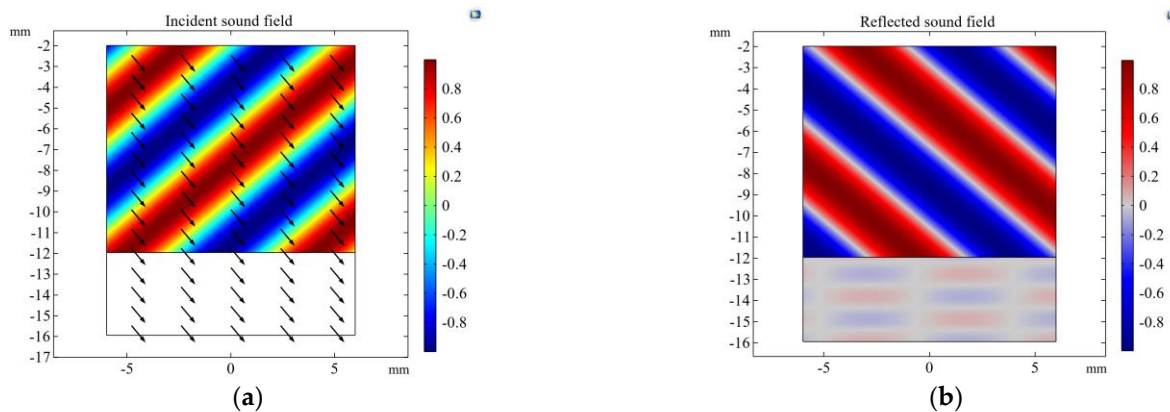


Figure 8. $f = 0.01$ MHz, $\theta = 40^\circ$. Acoustic field map: (a) incident sound field, (b) reflected sound field.

As shown in Figure 8, the maximum sound pressure amplitude of the incident wave was 1 when it entered the upper flange cover, indicated by the arrow direction. When the incident sound field entered the silicone gasket through the upper flange cover, scattering and transmission phenomena occurred.

A multi-angle measurement model was established to change the incident angle of the sound field and simulate the reflection spectra under different incident angles, as shown in Figure 9.

As shown in Figure 9, as the driving frequency increased, an extremely low point approaching 0 appeared in the ultrasonic reflection coefficients for all incident angles. Under the same frequency condition, a larger incident angle resulted in a higher ultrasonic reflection coefficient. Therefore, selecting an appropriate incident angle can reduce the sound field attenuation and improve the detection efficiency. For example, when the air layer thickness was $50 \mu\text{m}$ and the incident angle was 30° , the ultrasonic reflection coefficient dropped to its lowest value of 0.1 as the frequency increased to 4.11 MHz. This indicates that most of the incident sound waves were transmitted and there was almost no reflected wave generated. At this driving frequency, the sound wave resonated with the air layer. Near the resonant frequency, the reflection coefficient tended toward 0, which means there was no reflected sound wave produced. Far from the resonant frequency, the reflection coefficient tended toward 1, which meant that the sound wave was completely reflected.

In summary, for the same air layer thickness, as the incident angle increases, the resonant frequency also increases. However, in the detection process, large incident angles are not practical, and high-frequency sound waves attenuate rapidly during the propagation. Therefore, we set the incident angles to 10° , 20° , 30° , 40° , 50° , 60° , and 70° , and added a simulation comparison group with increased air layer thickness to improve the reliability of the calculation and facilitate the derivation of their relationship curve.

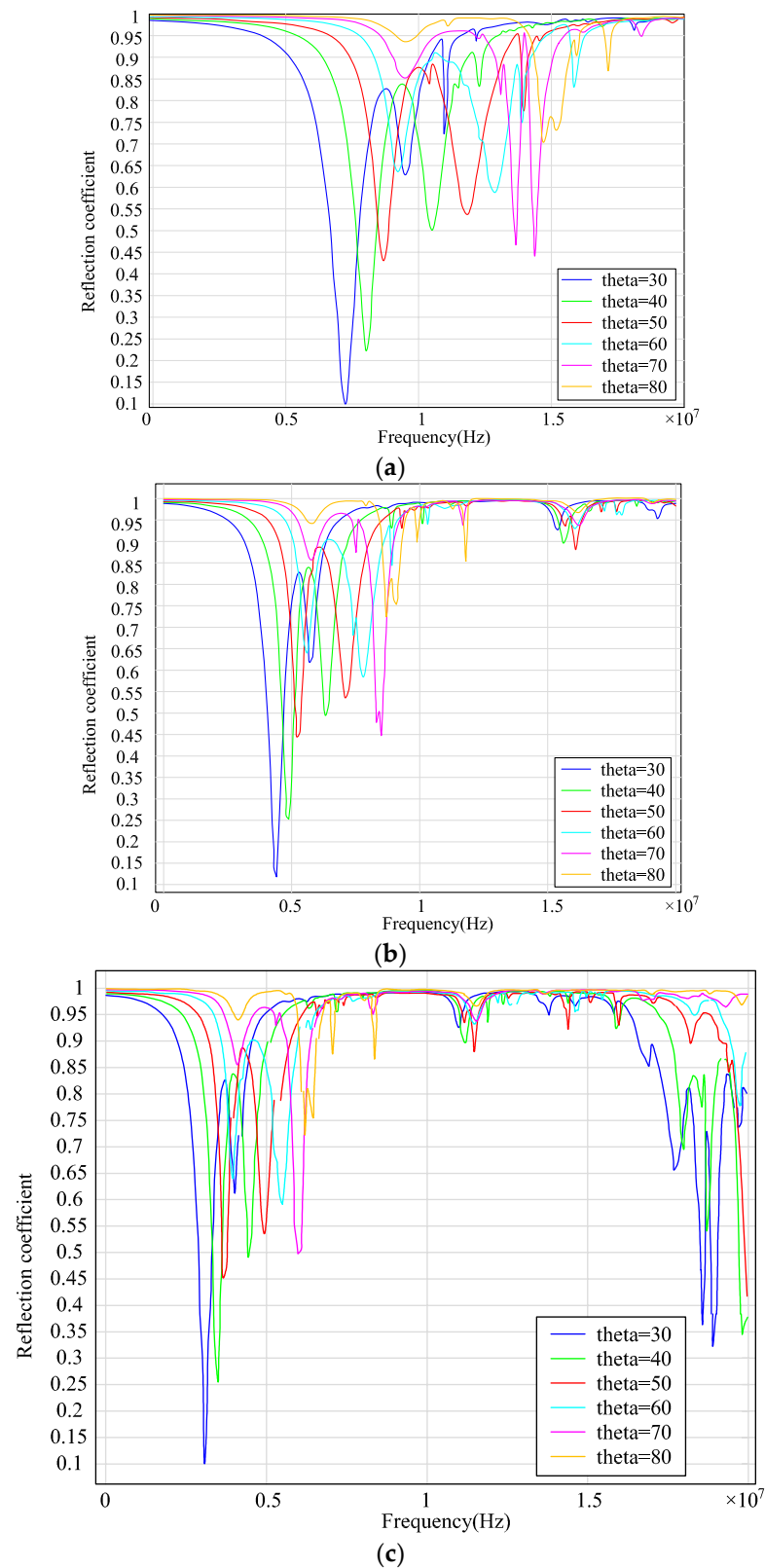


Figure 9. Reflection coefficient spectra under different air layer thicknesses and incident angles: (a) reflection coefficient spectra at $Q = 30 \mu\text{m}$, (b) reflection coefficient spectra at $Q = 50 \mu\text{m}$, (c) reflection coefficient spectra at $Q = 70 \mu\text{m}$.

4. Comparative Analysis of the Mathematical Model and Finite Element Model Results

4.1. Comparison of Results from the Vertical Incident of Sound Waves

In order to verify the accuracy of the model, it is necessary to compare the numerical results with those obtained from finite element simulations. Using the first-order resonance theory, the thickness of the air layer at different resonance frequencies was calculated and compared with the simulated results of the vertical incidence measurement model. The theoretical thickness of the air layer obtained by mathematical methods was obtained and is shown in Table 2.

Table 2. Data table for the extreme points of the reflection coefficient.

Air Layer Thickness Q/ μm	Reflectance Coefficient R	Resonance Frequency f/MHz	Theoretical Thickness Q/ μm	Deviation of Air Layer Thickness μm	Percentage Deviation of Air Layer Thickness %
30	0.013	5.61	30.6	0.6	2.0
50	0.067	3.41	50.2	0.2	0.4
70	0.024	2.41	71.1	1.1	1.5
90	0.114	1.91	89.7	0.3	0.3
110	0.049	1.51	113.6	3.6	3.2

The data in Table 2 represent a comparison between the results of the mathematical model and the finite element simulation model at the same frequency. The maximum deviation of the air layer thickness was 3.6 μm , with a deviation of 3.17%, and the minimum deviation was 0.3 μm , with a deviation of 0.3%, which is acceptable. The calculation nodes of the air layer thickness in the finite element simulation and the image of the first-order resonance theory curve for when the sound field was vertically incident are shown in Figure 10.

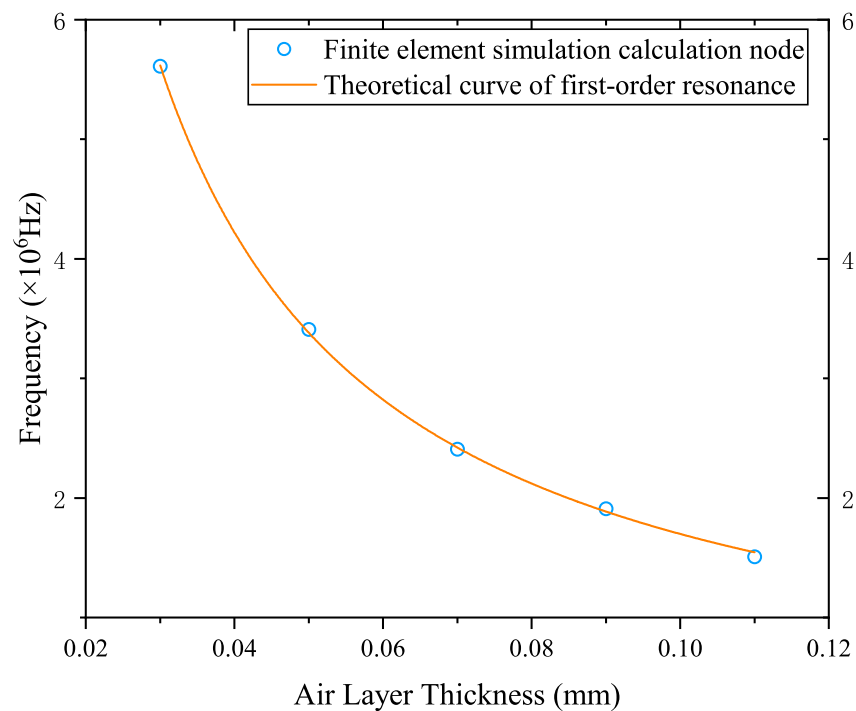


Figure 10. The relationship curve between air layer thickness and resonance frequency.

As shown in Figure 10, when the sound waves were vertically incident the air layer thickness nodes of the finite element model coincided with the resonance curve. This indicated that the vertical incidence model could be used to measure the air layer thickness in flange fastening devices. The first-order resonance frequency decreased as the air layer thickness between the flange cover and the silicone gasket increased. Moreover, when the air layer thickness tended to infinity, the first-order resonance frequency tended to infinity, and the two exhibited a power-law function relationship.

Based on the comparison between the results of the mathematical model and the simulation results of the finite element model, it was found that there was a good agreement between the finite element solution and the numerical calculation solution, which indicates that this model can be used to calculate the thickness of the air layer between flanges when ultrasonic waves are vertically incident. However, during the inspection process, due to the special nature of the structure of the flange fastening device and the service environment, the sound field cannot be vertically incident. Therefore, a multi-angle finite element measurement model was established to investigate the influence of air layer thickness on the first-order resonance frequency under different incidence angles.

4.2. Comparison of Results from the Multi-Angle Incident of Sound Waves

When the incidence angle of sound waves was non-perpendicular, the first-order resonance frequency of the air layer at different incidence angles and different thicknesses was calculated through COMSOL finite element simulation. The results are shown in Table 3.

Table 3. Numerical table of resonance frequencies at multiple angles.

Air Layer Thickness Q/ μm	Angle of Incidence ($^{\circ}$)						
	10	20	30	40	50	60	70
0.03	5.81	6.41	7.31	8.11	8.81	9.31	9.61
0.04	4.41	4.81	5.51	6.11	6.61	7.01	7.21
0.05	3.51	3.91	4.41	4.91	5.31	5.61	5.81
0.06	2.91	3.21	3.71	4.11	4.41	4.71	4.81
0.07	2.51	2.81	3.11	3.51	3.81	4.01	4.11
0.08	2.21	2.41	2.71	3.01	3.31	3.51	3.61
0.09	2.01	2.21	2.41	2.71	2.91	3.11	3.21
0.10	1.71	1.91	2.21	2.41	2.61	2.81	2.91
0.11	1.61	1.81	2.01	2.21	2.41	2.51	2.61

The first-order resonant theory model only provides the relationship between the thickness of the medium and the resonant frequency for vertical incidence, and the relationship between the thickness of the medium and the resonant frequency for inclined incidence is unknown. Figure 11 shows the resonant frequency curves for different incidence angles. It can be observed that the resonant frequency under the same air layer thickness followed a power law function, which was consistent with the trend of resonant frequency under vertical incidence. The resonant frequency under different incidence angles can be fitted and used as a resonant model for multi-angle conditions. The fitting resonant theory model curves for different incidence angles are shown in Figure 12.

Based on Figure 12, it can be seen that the fitted curve shows an increasing trend of the first resonant frequency with the increasing incidence angle of the sound wave at a constant thickness of the air layer. Therefore, it is recommended to use a low incidence angle for measurement in practical applications to reduce the attenuation of high-frequency sound waves and improve the detection efficiency. When the air layer thickness is relatively thin, using a wide-band ultrasound probe can collect more frequency-domain information, thus making the measurement results more accurate.

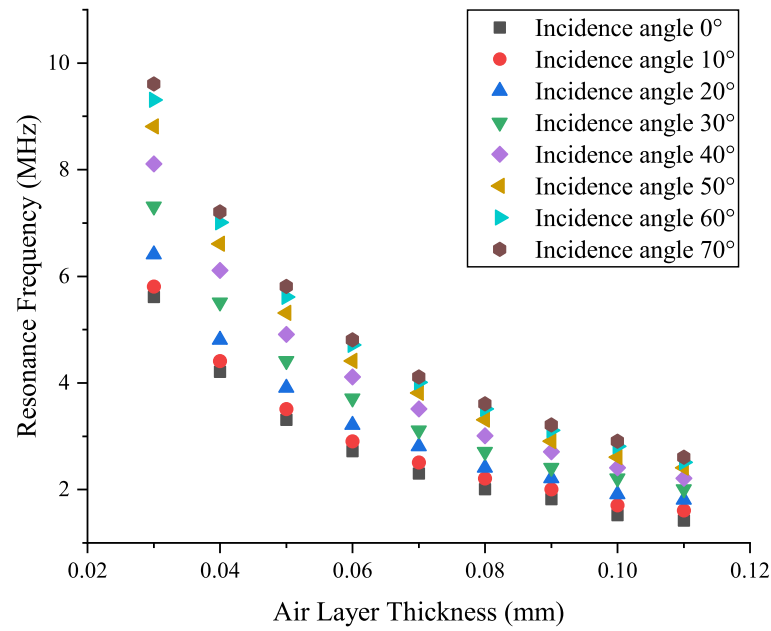


Figure 11. Resonance frequency points at multiple incidence angles.

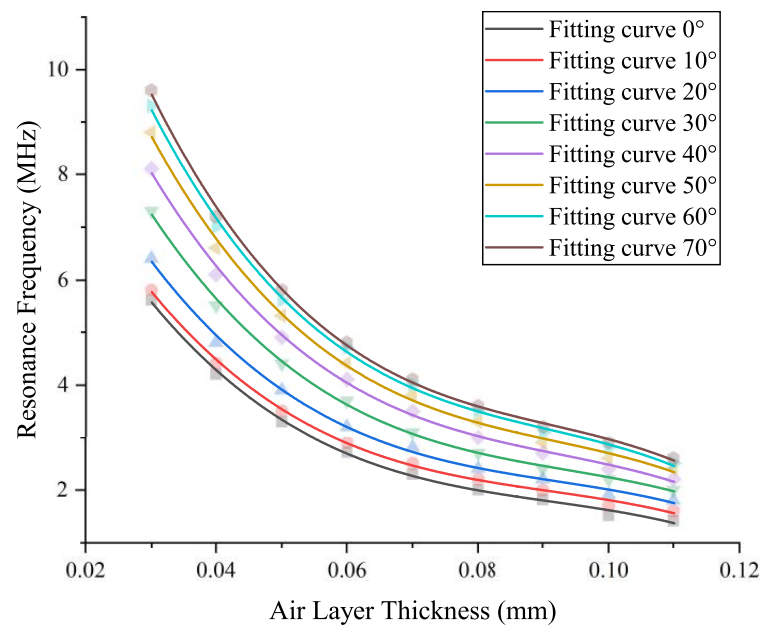


Figure 12. Resonance theoretical model curves for multi-angle incidence.

By fitting the simulated power function curves using MATLAB, the relationship between the first harmonic resonance frequency and the air layer thickness at different angles can be obtained as follows:

$$f(\theta) = kh^i \tag{12}$$

where θ is the incidence angle of the sound wave, k is the coefficient of the fitting curve equation, h is the thickness of the air layer, and i is the exponent term of the thickness of the air layer. The coefficients of Equation (12) obtained by fitting are shown in Table 4.

Table 4. Coefficients of the fitted curve equation.

Angle of Incidence (°)	0	10	20	30	40	50	60	70
Coefficient k	0.1715	0.1877	0.1993	0.2182	0.2392	0.2609	0.2776	0.2891
Exponent i	−1	−0.978	−0.992	−1.001	−1.007	−1.005	−1.003	−1

From Equation (12) and Table 4, it can be seen that the coefficients in Equation (12) increase with increasing incidence angle. Therefore, a function can be established to relate the coefficient k to the incidence angle θ , and the reflection coefficient under different incidence angles can be analyzed using the newly established fitting function. The graph of the fitting function and the coefficient k is shown in Figure 13.

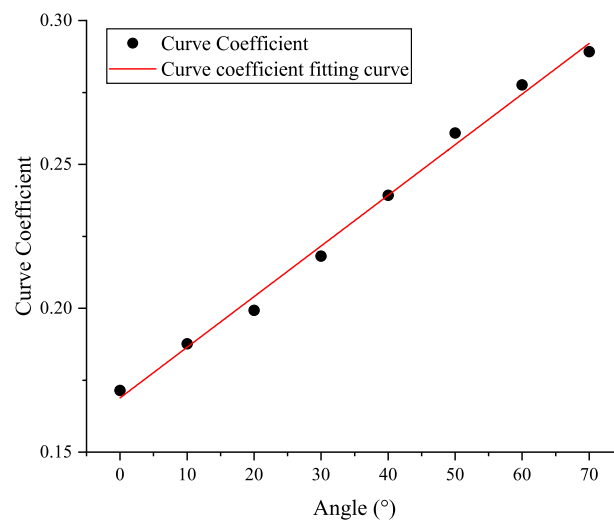


Figure 13. Relationship curve between curve coefficients and incidence angle and its fitting.

From the graph, it can be observed that the coefficient k follows a linear distribution. A linear function relationship can be established between the coefficient k and the incident angle θ , as shown in Equation (13).

$$k = 0.0018\theta + 0.1688 \tag{13}$$

According to Table 4, the exponential term in Equation (12) varies as a polynomial. The exponent i and its fitting curve are shown in Figure 14.

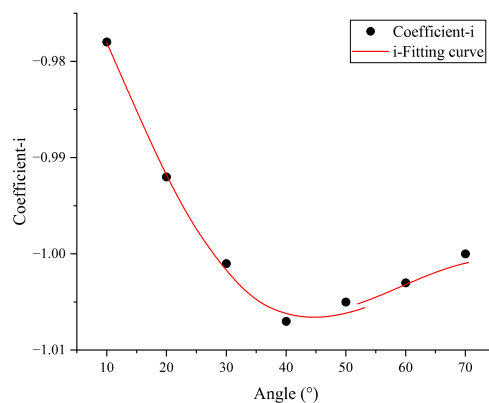


Figure 14. Fitting curve for the exponent term of the first-order resonant equation.

The fitting equation for the exponential term is:

$$i = 8.3333 \times 10^{-11}\theta^5 - 2.3106 \times 10^{-8}\theta^4 + 2.0719 \times 10^{-6}\theta^3 - 5.5416 \times 10^{-5}\theta^2 - 8.3530 \times 10^{-4}\theta - 0.9661 \quad (14)$$

The first harmonic resonance equation under multi-angle incidence can be obtained from Equations (13) and (14):

$$f(\theta) = (0.0018\theta + 0.1688)h^i \quad (15)$$

where $f(\theta)$ is the first-order resonant frequency equation.

To validate the reliability of the curve coefficient equation, numerical calculations and finite element simulations were conducted to obtain the first-order resonant frequency under four different operating conditions: air layer thickness of 0.03 mm and 0.05 mm, and incident angles of 15° and 45°. The results are shown in Table 5 for comparison and analysis.

Table 5. Resonant frequencies obtained from numerical and finite element simulations.

Type of Computation	Angle of Incidence (mm)	Air Layer Thickness (°)	
		0.03	0.05
Mathematical calculation	15	6.20	3.75
	45	8.52	5.09
Finite element analysis	15	6.11	3.61
	45	8.41	5.01

Based on Table 5, the first-order resonant frequencies obtained by fitting function and finite element simulation calculations were in good agreement for different operating conditions, with a minimum difference of 0.08 MHz and a maximum difference of 0.14 MHz. Therefore, the fitting function of the first-order resonant frequency can be applied to measure the thickness of the air layer under different incident angles, which indirectly characterizes the actual contact state between the flange and the silicone gasket.

When conducting curve fitting, the number of fitting points is limited and relatively small. Therefore, there exists an error between the values of the fitting curve and those of the fitting points. To reduce the interference caused by errors when calculating the reflection coefficient, an error analysis of the fitting curve is necessary. Considering the characteristics between the discrete points and the fitting curve, the RMS error analysis method was chosen, as shown in Equation (16).

$$X_{\text{RMSE}} = \sqrt{\frac{\sum_{i=1}^N (X_{\text{obs},i} - X_{\text{model},i})^2}{N}} \quad (16)$$

where X_{RMSE} is the RMS error value, $X_{\text{obs},i}$ is the observed value, $X_{\text{model},i}$ is the true value, and N is the number of observations.

The errors calculated according to Equation (16) are shown in Table 6. It can be concluded from the data in Table 6 that the fitting between the discrete points and the fitted curve was good, and the error can be ignored when calculating the thickness of the air layer through the fitted curve.

Table 6. RMS error value.

Figure	Error Value
Figure 4	0.01056
Figure 6	0.03343
	0.03101
	0.04741
	0.04716
	0.04303
	0.02933
	0.04291
0.04898	
Figure 10	0.00361
Figure 11	0.00138

5. Conclusions

Based on the consideration of the resonance frequency theory of the air layer in the incident ultrasonic wave, this paper solved the resonance conditions of different thicknesses of air layers at different frequencies using both mathematical and finite element models. The measurement problem of the air layer thickness between the flange contact interface was solved, and the following conclusions were drawn.

- (1) Under the condition of the vertical incidence of sound waves, by using the displacement and stress equations of longitudinal waves in solids and the reflection conditions of elastic waves on non-homogeneous interfaces, the expressions of air layer thickness in the flange model containing an air layer were obtained. Based on the boundary conditions of elastic waves, the ultrasound resonance frequency under different air layer thickness conditions was calculated.
- (2) Based on considering the resonance frequency theory of ultrasonic waves generated by the air layer, this paper derived the expression of the air layer thickness in the flange model with the help of displacement and stress equations of longitudinal waves in solids and the reflection condition of elastic waves at the interface of dissimilar media under the condition of vertical ultrasonic wave incidence. Based on the boundary conditions of elastic waves, the resonant frequencies of ultrasonic waves were calculated for different air layer thicknesses. Additionally, a finite element simulation model of the flange contact surface with an air layer was established. By simulating the pressure sound field distribution of reflection and transmission at different incident angles and frequencies, the angle and frequency spectra of ultrasonic reflection coefficients for different air layer thicknesses were extracted. Comparing the finite element results with the mathematical model results showed high consistency. The reliability of using the ultrasonic reflection coefficient method to evaluate the interface contact quality by measuring the air layer thickness was confirmed.
- (3) Based on the vertical incidence model, a multi-angle incidence air layer thickness measurement model was derived and constructed. The relationship between air layer thickness and incidence angle under multiple incidence angles was obtained. The influence of the ultrasonic incidence angle and air layer thickness on the resonance frequency of the air layer was analyzed in detail. The results showed that when the incidence angle was constant, the resonance frequency of the air layer gradually decreased as the air layer thickness increased in a power function form. When the air layer thickness was constant, the resonance frequency of the air layer gradually increased with increasing incidence angle. The thickness of the air layer between the flanges can be analyzed by the resonance frequency of the air layer at different incidence angles to infer the fitting degree of the flange contact surface and prevent leakage.

The above research results have led to the development of a multi-angle ultrasonic flange air gap thickness detection method which addresses the limitations of probe incidence angles in the detection of certain flange structures, ensures the operability of flange structure detection in any environment, and improves the accuracy issues caused by incidence angle limitations. This can provide technical and theoretical support for practical industrial applications.

Author Contributions: Conceptualization, F.S. and H.Z.; methodology, B.S.; software, B.S.; validation, F.S., H.Z. and B.S.; formal analysis, H.Z.; investigation, H.Z.; resources, F.S.; data curation, F.S.; writing—original draft preparation, H.Z.; writing—review and editing, B.S.; visualization, H.Z.; supervision, F.S.; project administration, H.Z.; funding acquisition, B.S. All authors have read and agreed to the published version of the manuscript.

Funding: This research was funded by the China National Natural Science Foundation, grant number 52075270, and by the Innovation Fund Project of Inner Mongolia University of Science and Technology, grant number 2017QDL-B08.

Institutional Review Board Statement: Not applicable.

Informed Consent Statement: Not applicable.

Data Availability Statement: Not applicable.

Acknowledgments: We are thankful for the support from the aforementioned funds.

Conflicts of Interest: The authors declare no conflict of interest.

References

1. Zhang, J.; Lian, Z.; Zhou, Z.; Song, Z.; Liu, M.; Yang, K. Leakage detection in a buried gas pipeline based on distributed optical fiber time-domain acoustic wave signal. *Eng. Fail Anal.* **2022**, *141*, 106594. [[CrossRef](#)]
2. Li, G. Establishment of Leakage Rate Model and Failure Analysis of Bolt Flange System. Master's Thesis, Kunming University of Science and Technology, Kunming, China, 2014.
3. Seyed, M.Y.N.; Masoud, G. Looseness Detection and Assessment of Flange Type Joints Using Vibroacoustic Modulation Method. *Russ. J. Nondestruct.* **2020**, *56*, 490–505.
4. Ishii, Y.; Biwa, S. Evaluation of interlayer interfacial stiffness and layer wave velocity of multilayered structures by ultrasonic spectroscopy. *J. Acoust. Soc. Am.* **2014**, *136*, 183–191. [[CrossRef](#)] [[PubMed](#)]
5. A study of the interaction between ultrasound and a partially contacting solid—Solid interface. *Proc. R. Soc. Lond. Ser. A Math. Phys. Eng. Sci.* **1997**, *452*, 2613–2628.
6. Wu, W. Research on the Air-Coupled Ultrasonic Testing of the Bonded Performance of Layered Medium. Master's Thesis, Jingdezhen Ceramic Institute, Jingdezhen, China, 2018.
7. Zilidou, M.; Smith, R.A.; Wilcox, P.D. Suppression of front and back surface reflections in ultrasonic analytic-signal responses from composites. *Ultrasonics* **2022**, *126*, 106815. [[CrossRef](#)] [[PubMed](#)]
8. Wang, X.; Wang, J.; Huang, Z.; Li, X. Measurement Interface Stiffness of Bonded Structures Using Air-Coupled Ultrasonic Transmission Technology. *IEEE Access* **2021**, *9*, 43494–43503. [[CrossRef](#)]
9. Li, X.; Ma, X.; Zhang, B. Theory and Numerical Calculation of Acoustic Reflection Coefficient for Oil Film Thickness Measurement. *Lubri. Eng.* **2018**, *43*, 13–18+27.
10. Geng, X.; Zhang, C.; Zhang, J.; Luo, G.; Shen, Q. Simultaneous measurement of layer thicknesses in thin layered materials using the phase of ultrasonic reflection coefficient spectrum. *Appl. Acoust.* **2022**, *195*, 108835. [[CrossRef](#)]
11. Dou, P.; Zou, L.; Wu, T.; Yu, M.; Reddyhoff, T.; Peng, Z. Simultaneous measurement of thickness and sound velocity of porous coatings based on the ultrasonic complex reflection coefficient. *NdtE Int.* **2022**, *131*, 102683. [[CrossRef](#)]
12. Shirgina, N.V.; Kokshaiski, A.I.; Korobov, A.I. Nonlinear Reflection of Elastic Waves from the Boundary of Solids. In Proceedings of the IEEE International Ultrasonics Symposium, Chicago, IL, USA, 3–6 September 2014.
13. Ding, J. Research on Measuring Method of Liquid Layer Thickness Based on Ultrasonic. Master's Thesis, Chongqing University, Chongqing, China, 2020.
14. Achenbach, J.D. *Wave Propagation in Elastic Solids*; Elsevier Science Publishers: Amsterdam, The Netherlands, 1973.
15. Tang, W.; Ma, X. The Research on Measuring Oil Film Thickness by Reflection Coefficients. *Lubri. Eng.* **2010**, *35*, 44–47.
16. Yu, M.; Reddyhoff, T.; Dini, D.; Holmes, A.; O'Sullivan, C. Using Ultrasonic Reflection Resonance to Probe Stress Wave Velocity in Assemblies of Spherical Particles. *IEEE Sens. J.* **2021**, *21*, 22489–22498. [[CrossRef](#)]
17. Cai, Y.; Fan, M.; Sun, P.; Xu, L.; Ma, J. Axial Super-Resolution Ultrasound Imaging With Quasi-Monopolar Pulses From a Dual-Frequency Transducer. *IEEE Trans. Instrum. Meas.* **2023**, *72*, 9500710. [[CrossRef](#)]

18. Gao, J.; Wang, X.; Lyu, Y.; Song, G.; Zhang, B.; He, C. Acoustic reflection and transmission at the interface between two-phase porous lithium-ion battery and liquid media. *Acta Acust.* **2023**, *48*, 138–147.
19. Stoll, R.D.; Kan, T.K. Reflection of acoustic waves at a water—Sediment interface. *J. Acoust. Soc. Am.* **1981**, *70*, 149–156. [[CrossRef](#)]
20. COMSOL Inc. *Acoustic Reflections off a Water-Sediment Interface*; COMSOL Inc.: Stockholm, Sweden; Available online: https://cn.comsol.com/model/download/1044311/models.aco.reflections_water_sediment.pdf (accessed on 1 November 2022).
21. Shukla, K.; Ahmad, A.; Ahluwalia, B.S.; Melandsø, F.; Habib, A. Finite element simulation of transmission and reflection of acoustic waves in the ultrasonic transducer. *Jpn. J. Appl. Phys.* **2022**, *61*, SG1029. [[CrossRef](#)]
22. He, C.; Li, Y.; Lyu, Y.; Song, G.; Wu, B. Ultrasonic reflection characteristics of FRP-to-FRP bonded joints with thick adhesive layers for bonding evaluation: Theoretical analysis. *Compos. Struct* **2020**, *246*, 112402. [[CrossRef](#)]
23. Fu, L.; Yang, M.; Sun, Y.; Tao, M. The Genetic Algorithm-Based Optimization Method for the Geometric and Material Parameters of Underwater Anechoic Coating. *IEEE Access* **2022**, *10*, 58030–58039. [[CrossRef](#)]
24. He, C.; Li, Y.; Lyu, Y.; Song, G. Finite element simulation of ultrasonic reflection/transmission characteristics for composite bonded joints with thick adhesive layers. *J. Beijing Univ. Aeronaut. Astronaut.* **2021**, *47*, 1721–1728.
25. Courant, R.; Friedrichs, K.; Lewy, H. Über die partiellen Differenzengleichungen der mathematischen Physik. *Math. Ann.* **1928**, *100*, 32–74. [[CrossRef](#)]
26. Liu, J. Research on Ultrasonic Testing Method of Adhesive Quality of Multilayer Structure Based on COMSOL. Master's Thesis, North University of China, Taiyuan, China, 2021.

Disclaimer/Publisher's Note: The statements, opinions and data contained in all publications are solely those of the individual author(s) and contributor(s) and not of MDPI and/or the editor(s). MDPI and/or the editor(s) disclaim responsibility for any injury to people or property resulting from any ideas, methods, instructions or products referred to in the content.